JOURNAL OF MATERIALS SCIENCE 28 (1993) 3173–3182

Electron-beam weld microstructures and properties of aluminium–lithium alloy 8090

A. RAVINDRA*, E. S. DWARAKADASA
Department of Metallurgy, Indian Institute of Science, Bangalore 560 012, India
T. S. SRIVATSAN
Department of Mechanical Engineering, The University of Akron, Akron, OH 44325, USA
C. RAMANATH, K. V. V. IYENGAR
Gas Turbine Research Establishment, C. V. Raman Nagar, Bangalore 560 022, India

Lithium-containing aluminium alloys are of considerable current interest in the aerospace and aircraft industries because lithium additions to aluminium improve the modulus and decrease the density compared to conventional aluminium alloys. Few commercial aluminium–lithium alloys have emerged for use in the aerospace industry. One such candidate is 8090, a precipitation-hardenable Al–Li–Cu–Mg alloy. The influence of electron-beam welding on the microstructure and mechanical properties of alloy 8090 material has been evaluated through microscopical observations and mechanical tests. Microscopic observations of the electron-beam welds revealed an absence of microporosity and hot cracking, but revealed presence of microporosity in the transverse section of the weld. Mechanical tests revealed the electron-beam weld to have lower strength, elongation and joint efficiency. A change in microscopic fracture mode was observed for the welded material when compared to the unwelded counterpart. An attempt is made to rationalize the behaviour in terms of competing mechanistic effects involving the grain structure of the material, the role of matrix deformation characteristics, grain-boundary chemistry and grain-boundary failure.

1. Introduction

Lithium-containing aluminium alloys have emerged as a family of attractive lightweight alternatives to traditional high-strength aluminium alloys and carbon-fibre composites for use in aerospace, automotive and marine applications. These alloys offer a unique combination of properties including high monotonic tensile and yield strength, decreased densities, increased stiffness, good resistance to the propagation of fatigue cracks, and improved thermal stability, coupled with the promise of attractive weight savings which would help lower operating costs by reducing fuel consumption [1]. For a large transport aircraft, a 1% reduction in weight translates into a 0.4% lower fuel consumption. For a large commercial aircraft this results in savings in fuel of around 33 000 gallons (150 018 l) a year [2]. In recent years, these alloys have aroused considerable scientific interest and have been the subject of increased research activity and several intensive investigations aimed at understanding their intrinsic metallurgical and mechanical performance characteristics [3–11].

Most high-strength aluminium alloys used in aircraft structures are mechanically fastened, which has the drawbacks of slow assembly and limitations in joining thin sections. Fusion welding of lightweight aluminium–lithium (Al–Li) alloys has been studied by a few investigators and has met with a limited degree of success [12]. However, there exists a critical need to develop new joining methods in order to extend the range of applications for these alloys and to improve the overall performance, durability, damage tolerance and life of safety-critical components and structures. Furthermore, new joining methods would facilitate use of these alloys in marine hardware, lightweight pressure vessels and lightweight commercial vehicles.

The economic benefits associated with the direct substitution and use of these alloys for conventional aerospace alloys resulted in the resurrection of considerable scientific and technological interest in developing new alloys that offered improvements in ductility, fracture behaviour, damage tolerance, moderate strength with corrosion resistance and ultrahigh strength [4–13]. This led to the emergence of ingot

---

* *Present address*: Department of Mechanical Engineering, The University of Akron, Akron, OH 44325, USA.

0022–2461

metallurgy alloys belonging to Al–Li–Cu–Zr and Al–Li–Cu–Mg–Zr systems. The commercial alloys from these systems are registered with the Aluminium Association as 2090 (Alcoa, USA), 2091 (Pechiney, France), 8090 and 8091 (Alcan's Laboratories, UK), and Weldalite™ 049 (Martin Marietta Laboratories, USA). Alloys 2090 and 8091 are considered as attractive high-strength alternatives for the Al–Cu–Zn–Mg (7XXX series) alloys, whereas, alloys 8090 and 2091 are projected as attractive alternatives for medium-strength and damage-tolerant applications replacing the existing Al–Cu–Mg (2XXX series) aluminium alloys, and Weldalite™ 049 for structural applications requiring weldability and high strength at cryogenic temperatures [13]. A major impediment to acceptance of these alloys was cost; somewhere in the neighbourhood of four times the cost of the aluminium alloys they were designed to replace.

Owing to the volatile nature of lithium, several problems arise and are associated during fusion welding of these alloys. These include: (a) porosity, (b) susceptibility to hot cracking, (c) loss of lithium and (d) loss of joint efficiency [12, 14]. Consequently, precautions need to be exercised to circumvent these problems. As sheets of an aluminium–lithium alloy are solution treated and artificially aged, after the finish-rolling operation, precipitation strengthening is lost in the weld metal. Hence, post-weld treatment becomes essential in order to improve the joint efficiency.

There have been only a few attempts to achieve a comprehensive understanding of the technique and use of welding to join alloy 8090. Pickens [13] and Skillingberg [15] documented the fusion-welding characteristics of alloy 8090 using gas tungsten arc welding (GTAW) technique. These studies revealed the alloy 8090 to have satisfactory weldability. However, the overall joint efficiency was low. On account of the high heat input associated with the GTAW technique, the amount of weld metal melted during the welding operation will be large, resulting in lithium depletion or dilution in the weld zone, coupled with the inducement of porosity. Furthermore, low penetration of the GTAW technique necessitates multiple passes in order to finish the weld operation. Each pass will tend to cause a change in the intrinsic microstructural features in the weld metal. The problems associated with fusion welding can be eliminated by the use of low heat input (high-intensity beam) and high penetration capability of the electron beam. With the aid of special jigs and tracers, welds of complex geometry can be produced using EBW, thus, making it an attractive fabrication technique. Bowden and Meschter [16] investigated the electron-beam weld solidification structures and properties of Al–3Cu–X alloys and found the weld zone to be weaker than the base metal. The weld specimens were observed to fail intergranularly, regardless of the overall composition of the matrix alloy. Le Poac *et al.* [17] evaluated the mechanical properties of electron-beam welds of alloy 8090. Gnanamuthu and Moores [18] used a laser welding process for the fusion joining of the 8090 alloy without using a filler material. They observed the quality of laser welds to be dependent on the surface preparation technique and highlighted the effect of laser parameters on the width of the heat-affected zone(HAZ). Other studies have examined the use of diffusion bonding and adhesive bonding as an attractive and viable means of joining the alloy [19, 20].

It is the objective of this study to evaluate the weldability characteristics of the Al–Li–Cu–Mg–Zr alloy 8090 joined by using the electron-beam welding technique. In particular, the influence of weld-bead orientation, with respect to the rolling direction, on mechanical properties was examined. The quality of the electron-beam weld was established through mechanical testing and microscopical observation of the weld.

2. Experimental procedure

2.1. Material

The aluminium–lithium alloy 8090 of composition (wt %) Al–2.8Li–1.3Cu–0.7Mg–0.12Zr (Table I) was provided by British Alcan Ltd, UK, in the T6 temper. The alloy was provided in the form of large rolled sheets of 1 mm thickness. The room-temperature mechanical properties of the as-received material are given in Table II. The T6 temper involved solution heat treatment at 480 °C for 1 h, and a cold-water quench. The as-quenched material was artificially aged at 180 °C for 24 h.

The iron and silicon elements in the alloy are impurities. During ingot solidification and subsequent processing, these impurities precipitate as insoluble constituent phases, Al_3Fe and Al_7Cu_2Fe. Zirconium

TABLE I Composition (wt %) of aluminium alloy 8090

Li	Cu	Mg	Zr[a]	Fe	Si	Zn	Ti	Al
2.8	1.3	0.7	0.12	0.05	0.02	0.03	0.03	Bal.

[a] Grain refiner, present as Al_3Zr.

TABLE II Mechanical Properties of Al–Li alloy 8090 in as-received condition

Temper	Test direction	0.2 % yield stress (MPa)	Tensile stress (MPa)	Elongation (%)	K_c (MPa $m^{1/2}$)
T6 typical	L	365	455	4.0	80
	T	375	465	7.5	60
T6 specimen min.	L	380	440	6.0	70
	T	380	440	6.0	70

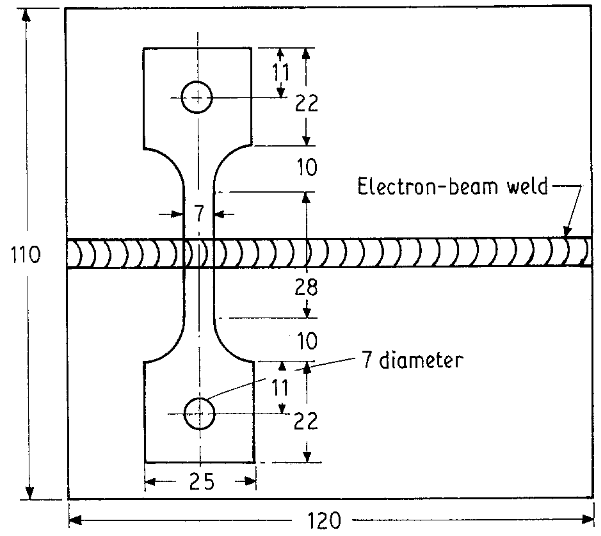

Figure 1 Transverse tensile weld specimen geometry and location of the weld bead with respect to the tensile stress axis.

addition results in the formation of metastable cubic $\mathrm{Al_3Zr}$ precipitates which are spherical in morphology and can effectively pin the grain and subgrain boundaries. The cubic $\mathrm{Al_3Zr}$ (β') phase, also known as dispersoid, has an $\mathrm{L1_2}$ crystal structure and nucleates heterogeneously on dislocations and grain boundaries [21, 22]. The dispersoid particle is coherent with the aluminium matrix and aids in retarding subgrain-boundary coalescence, suppressing recrystallization and controlling grain growth [23, 24]. The major strengthening precipitates in ternary Al–Li–Cu alloys are $\delta'(\mathrm{Al_3Li})$, $\mathrm{T_1(Al_2CuLi)}$, $\theta''(\mathrm{Al_2Cu})$ and $\theta'(\mathrm{Al_2Cu})$ [25–28]. In the peak-aged maximum-strength condition the Al–Li–Cu alloys contain precipitate-free zones (PFZs) along the grain and subgrain boundaries [27, 28]. Magnesium additions to ternary Al–Li–Cu alloy provides solid-solution strengthening and eliminates the formation of precipitate-free zones (PFZs) through the precipitation of S′ and S″ ($\mathrm{Al_2CuMg}$) phases near grain boundaries [29].

2.2. Microstructural characterization

Optical metallography samples were cut from the as-received sheet stock. The samples were cold mounted and wet ground on 320, 400 and 600 grit silicon carbide paper using water as lubricant and then mechanically polished using 1 μm alumina-based polishing compound. Grain morphology was revealed using Keller's etchant and observed in an optical microscope.

2.3. Electron-beam welding

Electron-beam butt welds were made on the as-received sheet-stock material (8090-T6). The welding was carried out in a vacuum chamber maintained at 10^{-4} torr (1 torr = 133.322 Pa). The welded plates were examined radiographically for internal flaws. Only radiographically acceptable welds were used for subsequent testing and analysis. Transverse weld tensile specimens were machined from the as-welded plates to measure the tensile properties. The geometry of the test specimen is shown in the Fig. 1. The

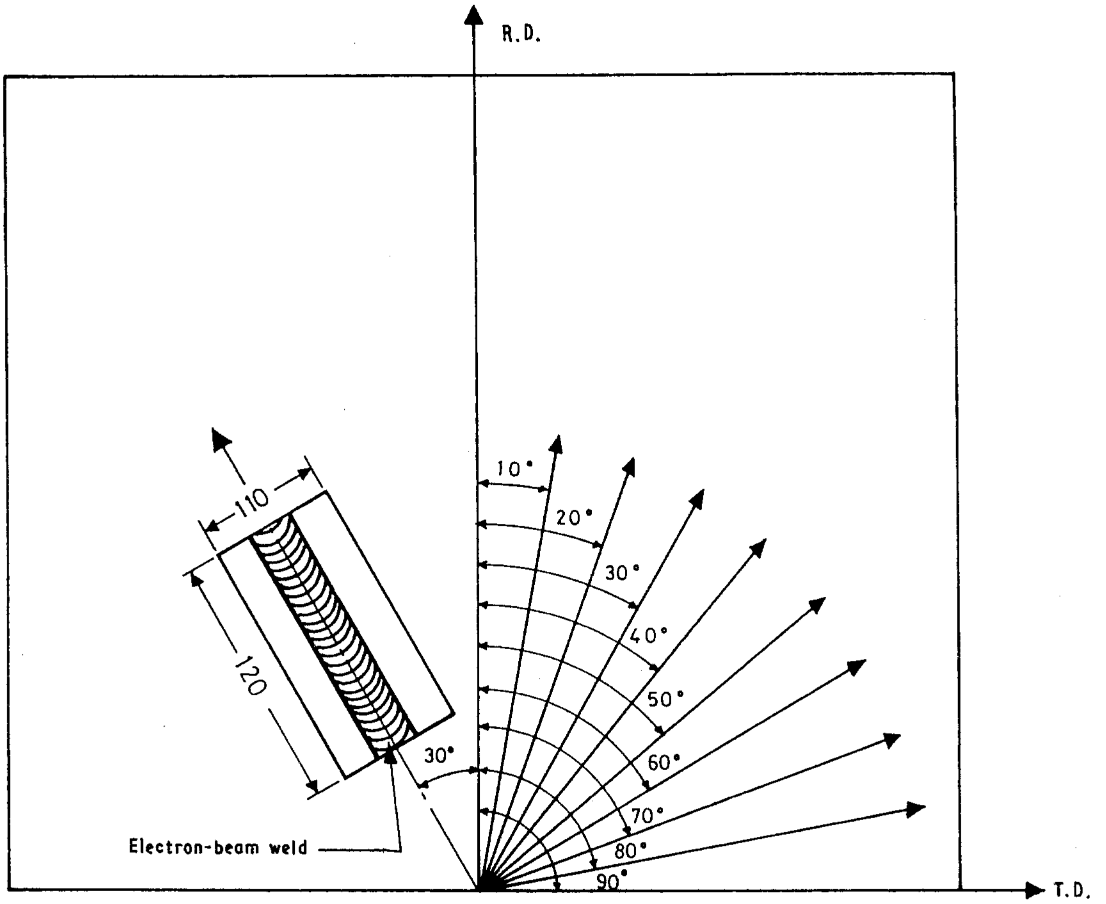

Figure 2 Schematic representation of the orientation of weld beads with respect to the rolling direction of alloy 8090 sheet.

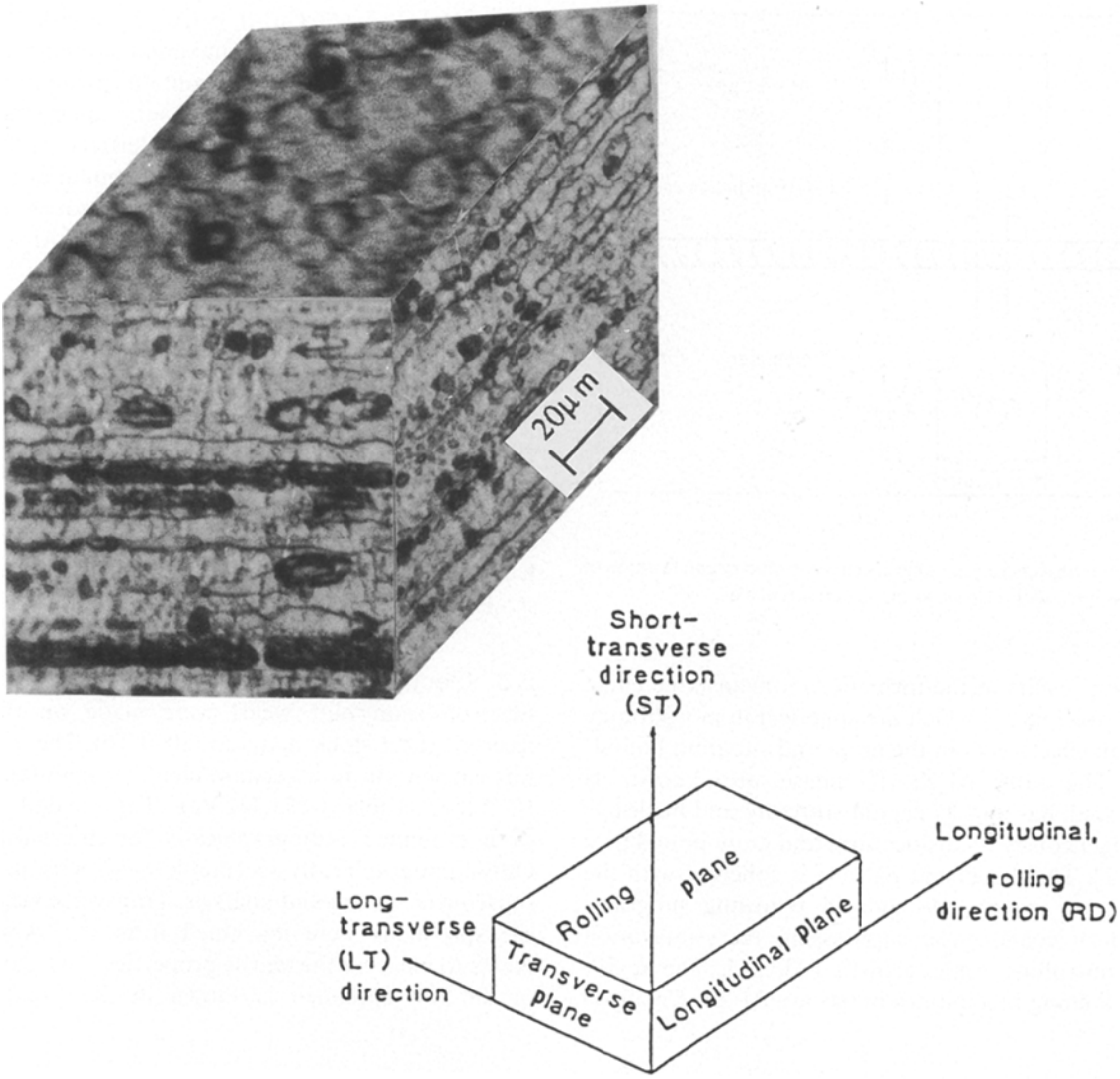

Figure 3 Optical microstructure of the alloy 8090-T6 illustrating pancake-type grain morphology.

specimens were chosen at intervals of 10 ° orientation of the weld bead with respect to the rolling direction of the as-received 8090 plate (Fig. 2).

Tensile tests were performed on a closed-loop servohydraulic testing machine. The tests were conducted at a constant crosshead speed of 0.07 mm s^{-1} (strain rate of $2.5 \times 10^{-3} s^{-1}$). Multiple tests were conducted in order to ensure consistency in results.

Fracture surfaces of the deformed tensile samples were examined in a scanning electron microscope (SEM) in order to determine the predominant fracture mode and to characterize the fine-scale fracture features.

3. Results and discussion

3.1. Initial microstructure

Microstructure of the as-received Al–Li–Cu–Mg–Zr alloy 8090 is shown in Fig. 3 as a triplanar optical micrograph illustrating the grain structure of the material in the three orthogonal directions (longitudinal, longitudinal-transverse and short-transverse). The material is partially recrystallized with the unrecrystallized grains flattened and elongated in the longitudinal direction, as a consequence of deformation introduced during rolling. The grain and subgrain boundaries were observed to be decorated with a fine dispersion of second-phase particles that are most likely: (a) the equilibrium phases $\{S(Al_2CuMg)$ and T-type $(Al_xCu_yLi_z)\}$; (b) the coarse iron-rich intermetallics; and (c) the magnesium-rich insoluble phase. In an earlier study [29], these particles were identified as: (i) the lithium-rich equilibrium phase $T_2(Al_6CuLi_3)$ that occurs in the form of massive rounded particles; and (ii) the equilibrium S (Al_2CuMg) phase. The anisotropic grain structure influences the mechanical behaviour of this alloy [30].

Weld metal exhibited a predominantly equiaxed grain structure in all three orthogonal directions (longitudinal, long-transverse and short-transverse) (Fig. 4). This is to be expected due to remelting of the alloy in the weld region. The fusion line was fine and narrow, with an almost complete absence of the heat-affected zone (HAZ) (Fig. 5). This is quite characteristic of the electron-beam welding technique. Small amounts of porosity were observed. The pores, of varying size, were isolated on the transverse plane. The grains at the centre region of the weld metal (Fig. 6a) were much larger in size than those at and near the fusion line (Fig. 6b). This observation is

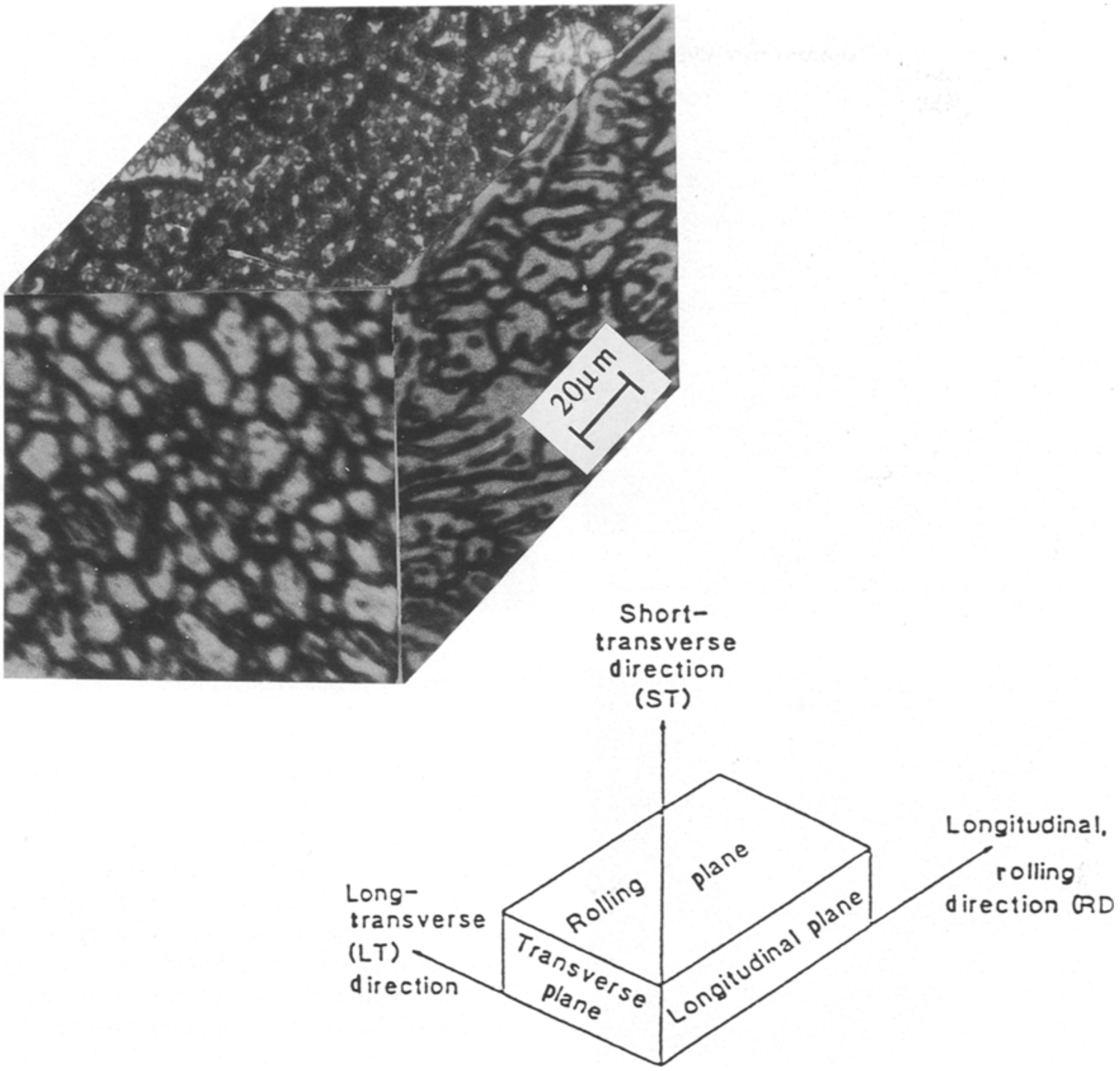

Figure 4 Optical microstructure of electron-beam weld indicating the cast microstructure.

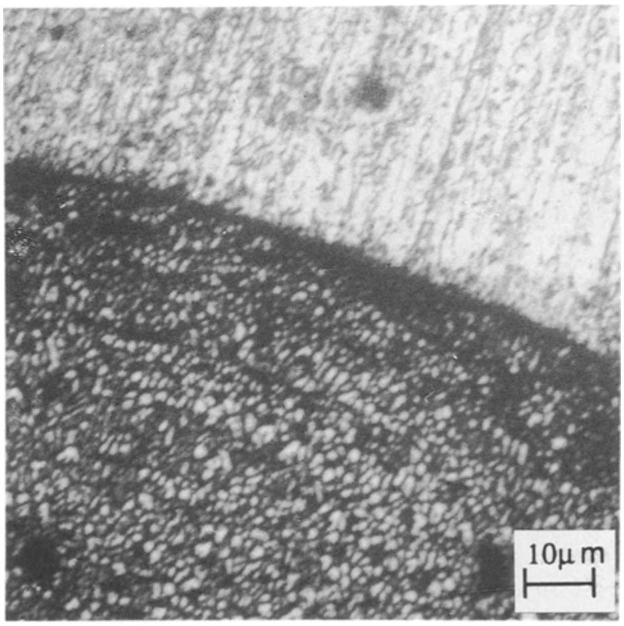

Figure 5 Optical microstructure of the weld indicating sharp fusion line and an almost absence of heat-affected zone.

unique, and is rationalized on the basis of the thermal cycle experienced by the weld bead. Also, the grains at and along the fusion line were observed to be oriented towards the centre of the weld and perpendicular to the welding direction (Fig. 7). This is attributed in part to the existence of large thermal gradients in the transverse direction of the weld compared to the longitudinal direction. Furthermore, the enhanced heat flux in the transverse direction when compared to the longitudinal direction, results in an orientation of grains in the transverse direction. Cross *et al.* [31] also observed and reported an oriented dendritic growth of grains in the weld metal due to the differential heat flux.

Etching with Keller's reagent revealed the grain boundaries of the weld metal to be more susceptible to enhanced and preferential attack than the grain boundaries of the as-received, unwelded material, that is, alloy 8090-T6. Mechanical and metallurgical properties of alloy 8090 are considerably influenced by grain-boundary structure and chemistry. Therefore, transmission electron microscope observations of the

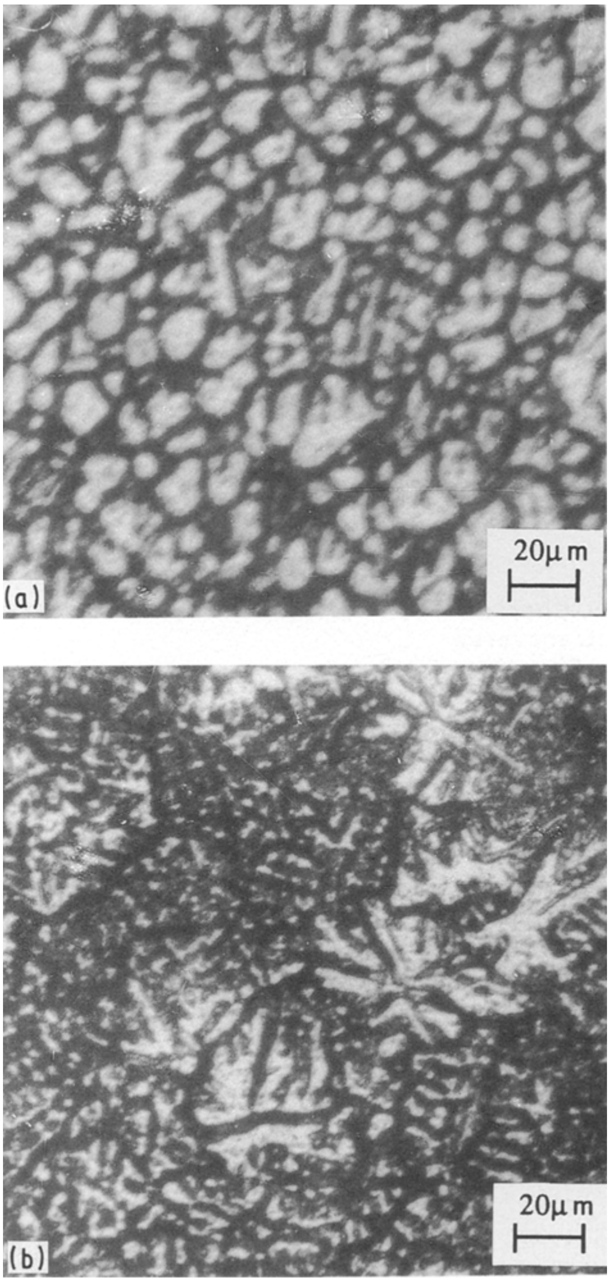

Figure 6 Optical microstructure of electron-beam weld metal (a) at the centre of the weld, (b) near the outer surface.

grain boundary are required in order to understand and elucidate the influence of grain-boundary chemistry on the performance characteristics of the alloy.

3.2. Radiographic examination

All the electron-beam welds that were radiographically examined indicated an absence of both macroporosity and hot cracking. However, at certain locations, the transverse section of the welds showed pores, of varying size, scattered across the surface. Hot cracking in the weld metal occurs due to the precipitation of low-melting point eutectics both at end along the grain and subgrain boundaries. These precipitates are unable to withstand the stresses arising from solidification shrinkage, resulting in the occurrence of hot cracks. Hot-cracking susceptibility is dependent on the conjoint action of several concurrent and competing factors, such as [14, 32] (a) joint restraint, (b) thermal gradients, (c) heat input, and (d) composition of the base metal. Even when all other factors are controlled, hot cracking can still occur due to intrinsic compositional variations between the base metal and weld zone. However, the presence of lithium has been found to have a beneficial influence on weldability because it does not favour the formation of the low melting point eutectics.

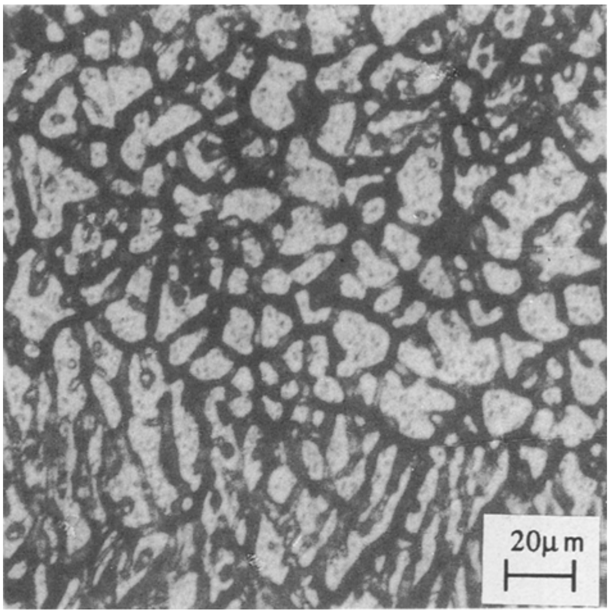

Figure 7 Optical microstructure of electron-beam weld metal illustrating orientation of grains towards the centre of weld.

3.3. Tensile properties

Tensile tests were conducted to identify the specific influence of weld microstructure on joint tensile strength, ductility and weld-joint efficiency. A comparison of the ultimate tensile strengths of the electron-beam weld and the as-received, unwelded material, that is, the base metal (aluminium alloy 8090-T6), for different orientations of the tensile stress axis with respect to the rolling direction, is shown in Fig. 8. The results reveal the tensile strength of the electron-beam weld to be consistently lower than that of the as-received, unwelded counterpart for all orientations of the tensile stress axis with respect to the rolling direction. The degradation in ultimate tensile strength of the welded sample was as high as 60% for the 0° oriented sample. Elongation to failure, ε_f, of the electron-beam welded specimens showed mixed response with orientations of the tensile stress axis. Along the rolling direction (0°) the ductility of the welded material was higher than that of the as-received, unwelded material. However, with increasing orientation of the tensile stress axis with respect to the rolling direction resulted in the electron-beam welded material having lower elongation than the unwelded base material (Fig. 9). The difference in elongation to failure between the as-received, unwelded and the welded material increased with orientation angle of the tensile stress axis with respect to the rolling direction, reaching a

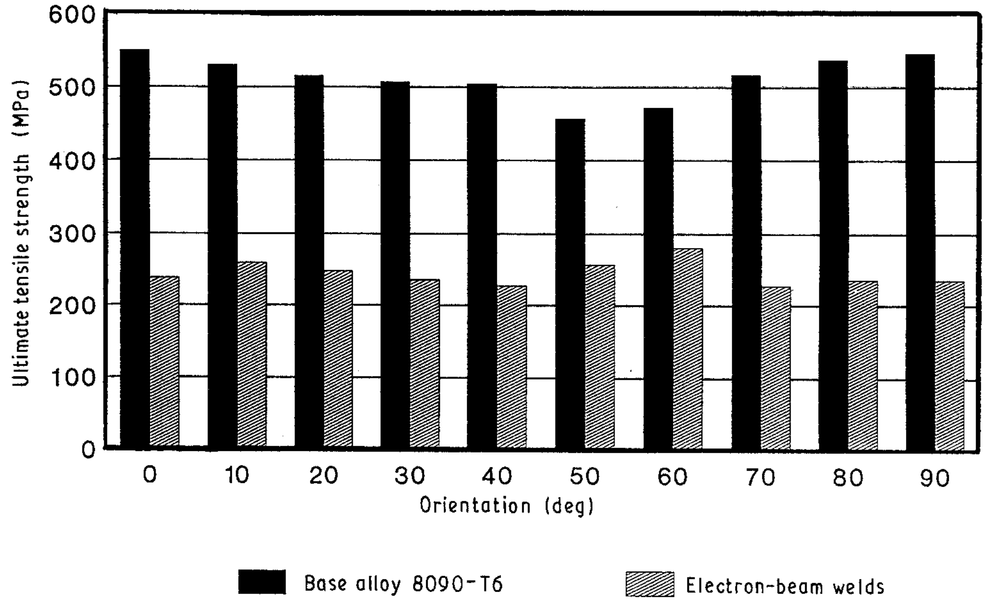

Figure 8 Tensile strength of the alloy 8090 and electron-beam welds as a function of orientation of stress axis with respect to the rolling direction.

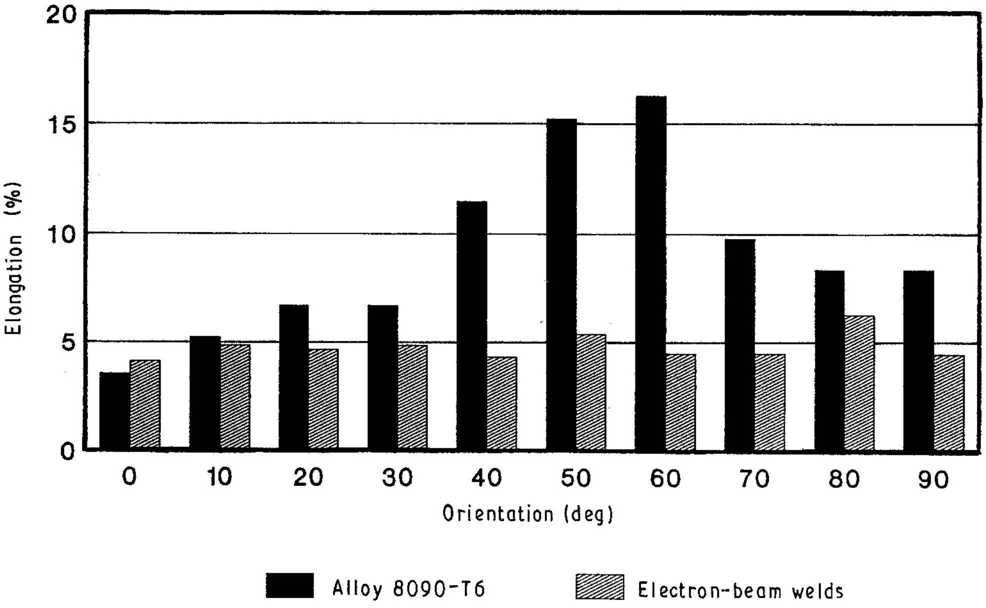

Figure 9 Per cent elongation of the alloy 8090 and electron-beam welds as a function of orientation of stress axis with respect to the rolling direction.

maximum for the 60 ° orientation. The welds prepared for the different orientation, however, revealed minimal difference and had a near reproducible quality. The ultimate tensile strength and elongation-to-failure of the electron-beam welds, as a function of orientation of stress axis, revealed consistency when compared to variations shown by the unwelded material. These results suggest the role of intrinsic microstructural effects and microstructural anisotropy in governing mechanical properties of the alloy. The anisotropy in properties exhibited by the as-received, unwelded material was not observed in the welded counterpart and is attributed to the microstructure of the weld metal.

The tensile strength joint efficiency for the welded conditions was measured shortly after welding. The joint efficiency was almost consistent at around 45% for most orientations reaching a maximum of 60% for the 60 ° oriented test specimen (Fig. 10). The low joint efficiency in almost all orientations prompted the need for post-weld heat treatment.

3.4. Fractography

To understand the fracture mode and to characterize the microscopic fracture features, all deformed samples were examined in a scanning electron microscope. Representative fractographs are shown in Figs 11–14. Tensile fracture of the as-received, unwelded material exhibited a predominantly mixed mode failure on a macroscopic scale. However, microscopic observations revealed fracture to be shear dominated. The sheared regions were oriented approximately 45 ° to the tensile stress axis, following a plane of maximum

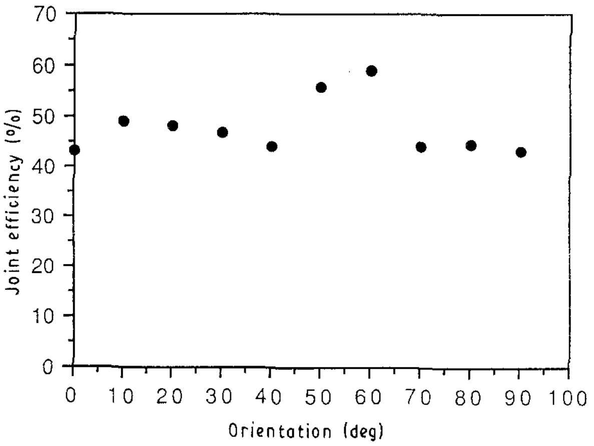

Figure 10 Joint efficiency of electron-beam welds computed as a function of orientation of stress axis with respect to the rolling direction.

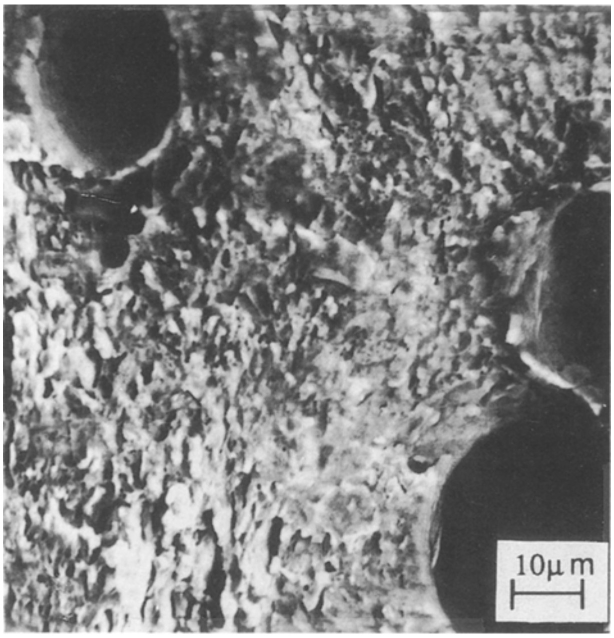

Figure 11 Scanning electron micrograph of tensile fracture of weld metal illustrating weld zone porosity for the 50° orientation sample.

macroscopic shear stress. The shear type of fracture tends to minimize necking and thus triaxial state of stress that occurs in a necked region [33]. Secondary cracks were observed on the fracture surface, separating the transgranular and intergranular regions, with the crack plane parallel to the major stress axis. The tendency towards localized inhomogeneous planar slip deformation results in strain concentration or localization at the point of impingement on the grain boundary. The high concentration of strain causes a large stress build-up at the grain boundary. Stress concentration accelerates the fracture process through (a) the initiation of microcracks at the grain boundary, and (b) voids at the coarse second-phase particles along the grain boundary. Fracture of the welded material was quite different from the as-received, unwelded material. Unlike a pancake grain morphology of the as-received (base) material the weld metal had a cast microstructure with relatively coarse grain size.

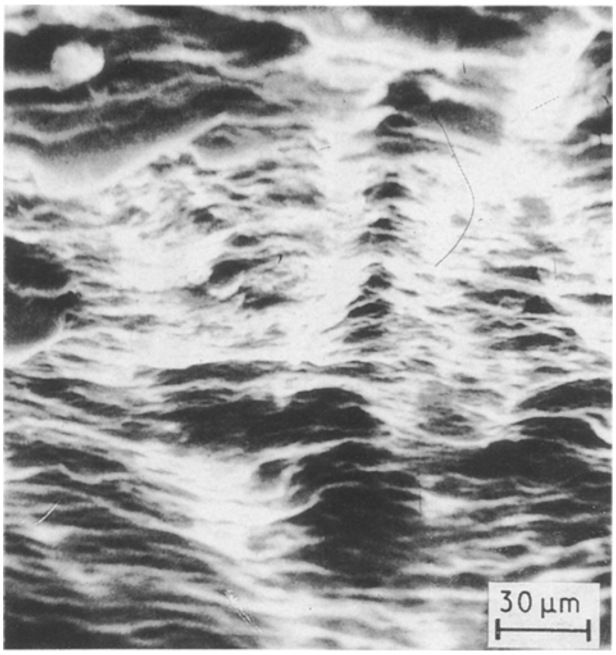

Figure 12 Scanning electron micrograph of tensile fracture of weld showing microvoid coalescence for the 0° orientation sample.

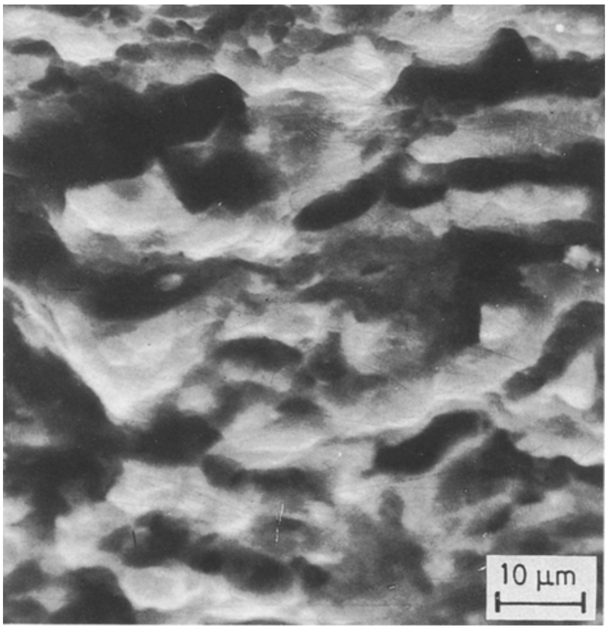

Figure 13 Scanning electron micrograph of tensile fracture of weld showing intergranular cracking and extensive microvoid linking in the vicinity of a pore for the 90° orientation sample.

Change in both grain size and morphology coupled with intrinsic changes in chemical composition of the grain-boundary regions is largely responsible for the observed difference in localized tensile fracture behaviour.

Fractographic analysis of the deformed electron-beam welded specimens revealed similar macroscopic fracture features for all orientations. The fracture plane was normal to the stress axis with a total absence of necking, thus, indicating the mode of failure for the welded samples to be brittle fracture. The occurrence of weld zone porosity is shown in Fig. 11. The general fracture surface features for the welds are

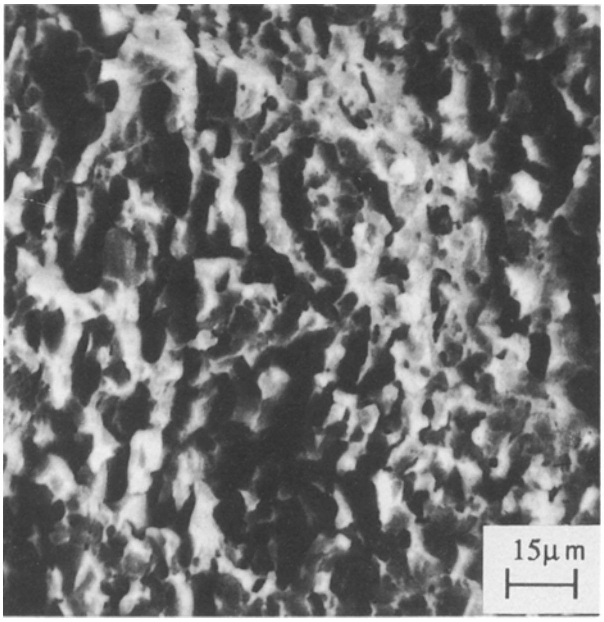

Figure 14 Scanning electron micrograph of the tensile fracture surface showing microvoid coalescence in the weld metal for the 50° orientation sample.

shown in Fig. 12 for the 0° orientation and Fig. 13 for the 90° orientation. Microscopic observations revealed microvoid coalescence (Fig. 14) and microcrack formation. Coalescence of microvoids was observed in the vicinity of a pore, which is a potential site for the initiation of microvoids. The microcracks result from stress-concentration effects at the grain boundary due to planar slip deformation.

4. Conclusions

1. Alloy 8090 is indeed weldable and radiographically acceptable quality electron-beam welds could be obtained.

2. The microscopic analysis indicated a dendritic growth of grains in weld metal. The grains at the centre of the electron-beam weld were larger compared to the grains in the outer surface.

3. The joint tensile strength efficiencies of the welds were found to be a function of orientation of stress axis with respect to the rolling direction. The joint efficiency was consistent and around 45%.

4. Variation in tensile strength and elongation was less for electron-beam weld metal compared to the unwelded strength and elongation of the material. The degradation in ultimate tensile strength was as high as 60%.

5. Fractographic analysis of the tensile fracture surface of the welds exhibited near similar features in all orientations. The fracture was comprised of extensive microvoid formation and coalescence with microcracking.

Acknowledgements

The authors thank the Aeronautical Research and Development Board, India for providing necessary funds (Grant Aero/RD-134/100/89-90/581) to carry out this work, and the University of Akron, Akron for providing partial support (T.S.S.) (Grant FRG 1101).

References

1. E. J. LAVERNIA, T. S. SRIVATSAN and F. A. MOHAMMED, *J. Mater. Sci.* **25** (1990) 1137.
2. JOHN MACK, *Mater. Engng* **7** (1988) 2.
3. P. A. MOLIAN and T. S. SRIVATSAN, *J. Mater. Sci.* **25** (1990) 3347.
4. T. H. Sanders Jr and E. A. Starke Jr (eds), "Aluminium–Lithium Alloys I", Proceedings of the First International Conference (Metallurgical Society, Warrendale, PA, 1983) p. 507.
5. *Idem*, "Aluminium–Lithium Alloys II", Proceedings of the Second International Conference (Metallurgical Society, Warrendale, PA, 1985).
6. S. J. Harris, C. J. Peel and P. J. Gregson (eds), "Aluminium–Lithium Alloys III", Proceedings of Third International Conference (Institute of Metals, London, 1987).
7. C. Champier, D. Dubost, S. F. Miannay and L. Sabetay (eds), "Aluminium–Lithium Alloys IV", Proceedings of the Fourth International Conference, J. de Phys. Coll., Vol. 3:6 France, 1987.
8. E. A. STARKE Jr, T. H. SANDERS Jr and I. G. PALMER, *J. Metals*, **12** (1981) 24.
9. P. J. GREGSON and H. M. FLOWER, *Acta Metall.* **33** (1985) 527.
10. T. S. SRIVATSAN and E. J. LAVERNIA, *J. Mater. Sci.* **26** (1991) 940.
11. E. S. BALMUTHU and R. SCHMIDT, "Aluminium–Lithium Alloys I", edited by T. H. Sanders Jr and E. A. Starke Jr (Metallurgical Society, Warrendale, PA, 1981) pp. 69–75.
12. J. R. PICKENS, *J. Mater. Sci.* **20** (1983) 4247.
13. J. R. PICKENS, F. H. NEUBAUM, T. J. LANGAN and L. S. KRAMER, in "Aluminium–Lithium Alloys V", Proceedings of Fifth International Conference, edited by E. A. Starke Jr and T. H. Sanders Jr (Materials Component and Engineering Publications, Birmingham, UK, 1989) p. 1397.
14. T. S. SRIVATSAN and T. S. SUDARSHAN, *Weld. J.* July (1991) 173-s.
15. M. H. SKILLINGBERG, in "Aluminium Technology '86", Proceedings of the Conference (Institute of Metals, London, 1986) p. 507.
16. D. M. BOWDEN and P. J. MESCHTER, *Scripta Metall.* **18** (1984) 963.
17. LE POAC, A. M. NOMINE and D. MIANNAY, in "Aluminium–Lithium Alloys I", Proceedings of Fourth International Conference, J. de Phys. Coll., Vol. 3:6 edited by G. Champier, B. Dubost, D. Miannay and C. Sabetay (1987) p. 293.
18. D. S. GNANAMUTHU and R. J. MOORES, in "Proceedings of Conference of Power Beam Processing" (ASM International, Metals Park, OH, 1988) p. 181.
19. M. R. EDWARDS, E. KLINKIN and V. E. STONEHAM, in "Aluminium–Lithium Alloys V", Proceedings of Fifth International Conference, edited by T. H. Sanders Jr and E. A. Strake Jr (Materials and Component Engineering Publications, Birmingham, UK, 1989) p. 431.
20. J. A. BISHOP, D. JOBLING and G. E. THOMPSON, in "International Conference on Advances in Joining and Cutting Processes", Abington, Cambridge, UK (Cambridge University Press, UK, 1990) p. 24.
21. E. NESS and N. RYUM, *Scripta Metall.* **5** (1971) 987.
22. R. J. RIOJA and E. A. LUDWICZAK, in "Aluminium–Lithium Alloys III", edited by C. Baker, C. J. Peel, S. Harris and B. Noble (Institute of Metals, London, 1985).
23. J. M. GALBRAITH, M. H. TOSTEN and P. R. HOWELL, *J. Mater. Sci.* **22** (1987) p. 27.
24. S. SURESH, A. K. VASUDEVAN, M. H. TOSTEN and P. R. HOWELL, *Acta Metall.* **35** (1987) 25.
25. J. M. SILCOCK, *J. Instit. Metals* **88** (1959–60) 957.
26. B. NOBLE and G. E. THOMPSON, *Metal Sci. J.* **6** (1972) 167.

27. K. SCHNEIDER and M. VON HEIMENDHAL, *Z. Metallkde* **64** (1977) 742.
28. T. S. SRIVATSAN, E. J. COYNE Jr and E. A. STARKE Jr, *J. Mater. Sci.* **21** (1986) 1557.
29. R. E. CROOKS and E. A. STARKE Jr, *Metall. Trans.* **15A** (1984) 1367.
30. T. S. SRIVATSAN and T. A. PLACE, *J. Mater. Sci.* **24** (1989) 1543.
31. C. E. CROSS, D. L. OLSON, G. R. EDWARDS and J. F. CAPES, in "Aluminium–Lithium Alloys-II", Proceedings of Second International Conference, edited by T. H. Sanders Jr and E. A. Starke Jr (Metallurgical Society, Warrendale, PA, 1985) p. 675.
32. J. A. VACCARI, *Amer. Machinist* February (1991) 50.
33. W. X. FENG, F. S. LIN and E. A. STARKE Jr, *Metall. Trans.* **15A** (1984) 1209.

Received 9 January
and accepted 20 November 1992